Attitude Dynamics and Stability Analysis of a Heliogyro Solar Sail

By Adonis PIMIENTA-PENALVER[1)], Li-Wei TSAI[2)]
Jer-Nan JUANG[3)], and John L. CRASSIDIS[4)]

[1)] *Graduate Student, Department of Mechanical & Aerospace Engineering. University at Buffalo, Amherst, NY.*
[2)] *Graduate Student, Department of Engineering Science. National Cheng Kung University, Tainan, Taiwan.*
[3)] *Honorary Professor, Department of Engineering Science, National Cheng Kung University, Tainan, Taiwan.*
[4)] *CUBRC Professor in Space Situational Awareness, Department of Mechanical & Aerospace Engineering. University at Buffalo, Amherst, NY.*

A heliogyro-type solar sail concept, HELIOS (High performance Enabling Low-cost Innovative Operational Solar sail), has been proposed and studied at NASA Langley Research Center as an alternative to deep space missions without the need for on-board propellant. A distributed-parameter approach was used to derive a set of partial differential equations for characterizing the HELIOS dynamic behavior of a spinning membrane blade in 1970s. Recently, a discrete-mass approach has facilitated a large amount of analysis on the spinning membrane blade. Both approaches produce identical frequencies for the same size of discretized model of the spinning membrane. However, further research is needed to characterize the stability of the structure under the projected range of orbital conditions. In this paper, we further improve upon the existing discrete-mass model, and we extend its application from a single membrane blade to a full description of the dynamics of the HELIOS system with multiple spinning membrane blades around a central hub. First, the representation of the motion of the blade is evolved from a system of dual coupling to become a fully-coupled description of the membrane dynamics. Then, the structural stiffness properties and the external forcing terms that proceed from the solar radiation pressure are derived and applied to the system. The flutter phenomenon, which could be significant evidence to determine the systems stability regions, is demonstrated through simulation. By collecting results from models consisting of an increasing number of point masses --and thus, increasing fidelity-- the convergent conditions for system instability (flutter) are determined. Additionally, the approximated dynamics of multiple-blade heliogyro structures are examined under the effect of solar radiation pressure. Findings confirm that additional active control actuation at the blade roots is needed to maintain structural integrity and perform attitude-changing maneuvers, while highlighting the need for careful sizing of the spacecraft hub in order to preserve a certain degree of stability.

Key Words: HELIOS, heliogyro, blade dynamics, flutter

Nomenclature

w	:	out-of-plane deflection
v	:	in-plane deflection
u	:	deflection along elastic axis
φ_i	:	ith segment twisting deflection
o_1,o_2,o_3	:	hub frame rotation (gen. coordinates)
$\omega_x,\omega_y,\omega_z$	:	body frame axes rate (quasi-coordinates)
E	:	Young's modulus
G	:	Torsional rigidity
m_h	:	hub mass
r_h	:	radius of cylindrical hub
h	:	height of cylindrical hub
m	:	point mass
r	:	length of segment
s	:	blade half-width
R_i	:	position of the ith point mass
ρ	:	hub position in inertial frame
ω_0	:	nominal spin rate
w_s	:	constant out-of-plane deflection
f_{ni}	:	ith segment normal resultant of SRP force
SRP	:	Solar radiation pressure

Subscripts

I,H,R,B	:	inertial, hub, root, and body frames

1. Introduction

Perhaps predictably, studies on heliogyro blade dynamics draw heavily on helicopter rotor theory to formulate a distributed-parameter approaches. McNeal [1)] presents an analytical model of uncoupled beam equations to characterize the bending and twisting motions; thus establishing some results that have since served as baseline for evaluating dynamic models. Dowell and Hodges [2)] compare several methods of deriving equations of motion for rotor blades. Their formulation is extended to heliogyro blades by Gibbs and Dowell [3)] to predict flutter instabilities at low levels of solar radiation pressure (SRP). Similarly, Natori, Nemat-Nasser, and Mitsugi,[4,5)] investigate the convergence properties of a mixed-variational approach on helicopter blades with low torsional stiffness and predict flutter for thin flexible blades under SRP. Recent research is focused on the identification of the structure's dynamic behavior using approximated models. Such is the endeavor of Scholz, Hsiao, and Juang [6)] to study the deployment process using a lumped-mass approximation of a blade. Juang, Hung, and Wilkie [7)] study the principal frequencies of a discretized model of the uncoupled motions of a single heliogyro blade; while Huang, Juang, Hung, and Wilkie,[8)] apply and validate the same discretizing approach to scaled models under gravitational and centrifugal loads.

The present study attempts to improve the computationally-friendly discretized models with the fidelity of distributed parameter approaches by incorporating structural stiffness properties onto the lumped-mass approximations of the blade. Initial work along this vein has already been carried out,[9] where the stability of the blade --and thus, flutter-- is investigated at differing levels of solar radiation pressure and spin rates. As a prolongation of the work in reference 10, the present investigation also employs a hybrid-coordinate approach, following the formulation by Meirovitch,[11] to represent the full heliogyro by adding a continuous hub to the discretized blades.

Not unlike helicopters, the stability and attitude control in all six degrees of freedom of the heliogyro is achieved through the coordination of three pitching profiles: collective, cyclic, and half-pitch. Blomquist [12] compares blade modeling approaches and ultimately finds that, under some limiting conditions, a root controller for the blade pitch can completely control the thrust vector of a heliogyro. Juang, Lu, Horta, and Wilkie,[13] demonstrate time and frequency-domain system identification methods utilizing synthetic data and introduce preliminary controller design. Their investigation remarks the need for a pitch controller which is driven toward a more complete dynamic model in order to achieve acceptable levels of damping. Guerrant, Lawrence, and Wilkie [14,15] have devoted efforts to developing approximate models for the blade twist dynamics and establishing control strategies to perform collective and cyclic maneuvers. Guerrant and Lawrence [16] then apply a nonlinear optimization approach to establish a set of pitch profile combinations designed to achieve any desired control forces, or moments, in varying mission scenarios. Furthermore, Guerrant [17] also studies the blade's structural dynamics, heliogyro orbital performance, and shows that the spacecraft should be fully controllable in all flight conditions.

A common denominator among previous control research on heliogyros is the conclusion that the controllers must be driven toward models that capture more of the dynamic characteristics of the flexible blades. With regards to stability and control, this paper presents a simulation-based study of the approximate structural dynamics of the full heliogyro structure under the effects of solar radiation pressure and control command, the latter of which consists of actuating motors at the blade roots to change blade pitching, and reaction wheels to affect the hub's orientation. It is the desire of the investigators to showcase a computationally friendly manner of obtaining heliogyro equations of motion while reproducing as many dynamic effects as possible. Designing controllers based on this model should provide a better idea of what is realistically possible in orbital conditions.

This article is organized as follows: Section 2 presents the system formulation, which includes the position and velocity of the discretized masses, the Lagrangian-based derivation of the equations of motion, the external forcing from actuation and solar radiation pressure, as well as the nominal static deflection on the blades. Simulation results on the dynamics and stability of a single blade are given in section 3.1. Furthermore, sections 3.2, 3.3, and 3.4 present results from the 1-blade+hub, 2-blade+hub, and 4-blade+hub systems, respectively. A final summary of the findings of this paper is given in section 4.

2. Attitude System Formulation

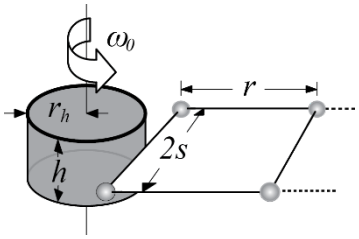

Fig. 1. Hybrid model: continuous hub + discrete masses.

The model presented in this paper is heavily influenced by that of reference 7. In that paper, their approach consists of dividing the blade into equal sections, where the total mass is proportionally lumped into discrete points located at the edges of these sections; the point masses are separated from each other by massless, but rigid rods. The properties of that model are largely preserved in this paper except that, now, the elastic deformations in references 2 and 3 are re-defined as linear coordinates and conformed into the rigidity of the lumped-mass model. In contrast with the discretizing approximation of the blade, the hub of the heliogyro is given the shape of a thick disk of mass m_h, radius r_h and thickness h; this is done in full conscience of the fact that the actual mass distribution of the hub in a real mission would depend on the arrangement of the bus instruments and the inertia of each with respect to the center of rotation. Figure (1) depicts the pertinent system dimensions.

A set of variables, which measure elastic deformations, has been defined to describe the dynamics of each section of the blade; they are shown in figure 2. Their formulations are similar to those presented by Dowell, Gibbs, and Hodges [2,3] which are defined on axial (u, v, and w, for the x, y, and z directions, respectively) and torsional (φ) elastic deformations due to stress and strain. It is important to note that these generalized coordinates are defined in each segment's rotational frame.

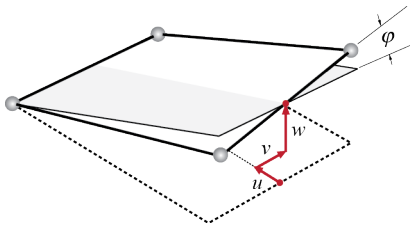

Fig. 2. Dowell & Hodges' deformations.

The generalized coordinates are collected in Eq. (1). The axial deformation (u) is ignored entirely in this definition because, as it turns out, it can be defined entirely in terms of w, v, and r. Note that n_b and n refer to the number of blades in the heliogyro, and the number of segments per blade, respectively.

$$q = [w \quad v \quad \varphi \quad ...]^T \tag{1}$$

2.1. Position formulation

For reference, figure 3 shows the coordinate systems utilized hereafter: the segment-fixed blade coordinate systems for each section ($[e_{xi}, e_{yi}, e_{zi}] \in B$, in red), the root frame ($[e_{xr}, e_{yr}, e_{zr}] \in R$, in green) which is fixed to the actuator, the body-fixed hub coordinate system ($[e_x, e_y, e_z] \in H$, in blue), as well as a representative inertial manifold ($[e_X, e_Y, e_Z] \in I$, in black).

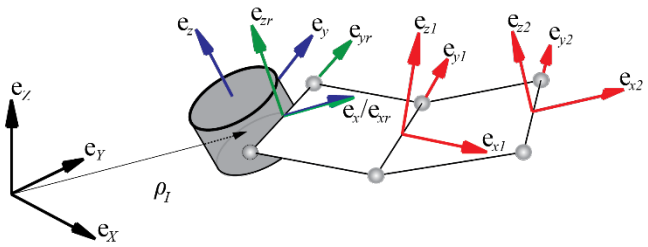

Fig. 3. Blade (red), root (green), hub (blue), and inertial (black) frames

For convenience, the position of the tip masses are defined using Dowell & Hodges deformations (Fig. (4)) as opposed to using the system's own dimensions (Fig. (3)). Eq. (2) shows the position of a tip mass using the deformation coordinates of Eq. (1). The mapping from the i^{th} blade frame B to the root frame R is carried out by T_{RB}, which is given in Eq. (3), while the conversion from the root frame to the hub (body) frame is shown in Eq. (4), where θ represents the pitching angle applied at the root by the actuating motor.

$$R_i = [\rho_X \quad \rho_Y \quad \rho_Z]_I^T + T_{HR}T_{RB}[r \quad s \quad 0]_I^T + R_{(i-1)H} \tag{2}$$

$$T_{RB} = \begin{bmatrix} 1 & 0 & 0 \\ 0 & \cos\varphi & \sin\varphi \\ 0 & -\sin\varphi & \cos\varphi \end{bmatrix} \begin{bmatrix} \frac{\sqrt{r^2-w^2}}{r} & 0 & \frac{w}{r} \\ 0 & 1 & 0 \\ -\frac{w}{r} & 0 & \frac{\sqrt{r^2-w^2}}{r} \end{bmatrix} \tag{3}$$

$$\begin{bmatrix} \frac{\sqrt{r^2-w^2-v^2}}{\sqrt{r^2-w^2}} & \frac{v}{\sqrt{r^2-w^2}} & 0 \\ -\frac{v}{\sqrt{r^2-w^2}} & \frac{\sqrt{r^2-w^2-v^2}}{\sqrt{r^2-w^2}} & 0 \\ 0 & 0 & 1 \end{bmatrix}$$

$$T_{RB} = \begin{bmatrix} 1 & 0 & 0 \\ 0 & \cos\theta & -\sin\theta \\ 0 & \sin\theta & \cos\theta \end{bmatrix} \tag{4}$$

2.2. Energy formulation

After deriving the velocities of the point masses using the transport theorem on Eq. (2) about the body rates ω_x, ω_y, and ω_z the kinetic and potential energies of the system can be understood as follows:

$$T = \frac{m}{2}\left(\sum_{i=1}^{n}(\dot{R}_i \cdot \dot{R}_i)\right) + \frac{I_{xx}\omega_x^2 + I_{yy}\omega_y^2 + I_{zz}\omega_z^2}{2} \tag{5}$$

$$V = \sum_{i=0}^{n}\left(\int_{-s}^{s}\frac{E\epsilon_{xx}^2 + G\epsilon_{xz}^2}{2}dy\right) \tag{6}$$

With regards to the potential energy of the attitude system, the present study attempts to incorporate elements of beam theory to account for some of the dynamics which might not be observable using a pure lumped-mass approximation. To this end, the deformations of the real blade --modelled as a very thin cantilever beam-- can be projected onto the sectional displacements of the lumped mass representation; the underlying assumption being that the in-plane, out-of-plane, and twisting motions can be thought of, respectively, as the translational and torsional vibrations of a fixed-free cantilever beam. In Eq. (6), the quantities E and G are the young's modulus and torsional rigidity of the blades, respectively; also, ϵ_{xx} represents the axial strain, while ϵ_{xy} and ϵ_{xz} represent the shear strains. In order to obtain an approximation of these quantities, the relative displacements on the e_{xi}, e_{yi}, and e_{zi} directions must be defined. Following references 2 and 9, these are $\bar{u}, \bar{v}$, and $\bar{w}$, respectively. Additionally, $\bar{\phi}$ corresponds to the total angle of twist along the elastic axis (e_{xi}). Figure 4 depicts the aforementioned relative displacements. Note that, since we assume symmetry about the elastic axis (e_{xi}) of each segment, either point mass can be used to define the twist deformation.

$$\begin{matrix} \bar{w}_i = R_H(z)|_{s=0} \\ \bar{v}_i = R_H(y)|_{s=0} \\ \bar{u}_i = R_H(x)|_{s=0} - i \cdot r \\ \bar{\phi}_i = \varphi_i + \varphi_{i-1} + \cdots \end{matrix} \quad \text{with} \quad \begin{matrix} \bar{w}_0 = 0 & \bar{v}_0 = 0 \\ \bar{w}_0' = 0 & \bar{v}_0' = 0 \\ \bar{w}_n'' = 0 & \bar{v}_n'' = 0 \\ \bar{\phi}_0 = 0 & \bar{\phi}_n' = 0 \end{matrix} \tag{7}$$

Forward and backward finite difference approximations are used to formulate the spatial derivatives of these quantities:

$$\begin{matrix} \bar{w}_i' = \frac{\bar{w}_i - \bar{w}_{i-1}}{r} & \bar{w}_i'' = \frac{\bar{w}_i' - \bar{w}_{i-1}'}{r} \\ \bar{v}_i' = \frac{\bar{v}_i - \bar{v}_{i-1}}{r} & \bar{v}_i'' = \frac{\bar{v}_i' - \bar{v}_{i-1}'}{r} \\ \bar{u}_i' = \frac{\bar{u}_i - \bar{u}_{i-1}}{r} & \bar{\phi}_i' = \frac{\bar{\phi}_{i+1} - \bar{\phi}_i}{r} \end{matrix} \tag{8}$$

The strains on the membrane, provided it is imagined as a very thin rotor blade, are approximated in Eq. (9), where y represents an arbitrary position along the blade cross-section.

$$\begin{matrix} \epsilon_{xx} = \bar{u}_i' + \frac{\bar{v}_i'^2 + \bar{w}_i'^2 + y^2\bar{\phi}_i'^2}{2} \\ -\bar{v}_i''(y\cos\bar{\phi}_i) - \bar{w}_i''(y\sin\bar{\phi}_i) \\ \epsilon_{xy} = 0 \quad \epsilon_{xz} = y\bar{\phi}_i' \end{matrix} \tag{9}$$

2.3. Lagrangian approach with hybrid coordinates

Following the Lagrangian approach ($L = T - V$), the equations of motion that describe the blade behavior may obtained using Eq. (10). Eq. (11) is the corresponding form of Lagrange's equation in terms of quasi-coordinates as presented by Meirovitch,[11] that is, the body angular rates ω_x, ω_y, and ω_z are utilized in place of the generalized coordinate rates $\dot{o}_1, \dot{o}_2$, and $\dot{o}_3$. This is done for the sake of convenience, as it is easier to formulate the kinetic energy, as well as any form of feedback control law, based on angular velocities about orthogonal body axes x, y, and z.

$$\frac{d}{dt}\left(\frac{\partial L}{\partial \dot{q}}\right) - \frac{\partial L}{\partial q} = \tau_q \tag{10}$$

$$\frac{d}{dt}\left(\frac{\partial L}{\partial \omega}\right) - [\Omega\times]\frac{\partial L}{\partial \omega} - B^T\frac{\partial L}{\partial o} = B^T\tau_o \tag{11}$$

In the preceding equations, the torques applied onto each of the generalized coordinates, including the body rates, are given by τ_q and τ_o. According to mission specifications, the only available inputs are reaction wheel, and pitching torques at the root of each blade. Furthermore, $[\Omega\times]$ represents the cross-product matrix of the body rates (ω_x, ω_y, and ω_z). The quantity B stands for the kinematic matrix associated with the particular Euler angle rotation utilized to convert from the hub (body) frame to an inertial frame. For the purposes of this analysis, a 3-2-1 rotation is utilized, which suggests that, for small angles o_1 and o_2, the quasi-coordinate rates can be approximated as the generalized-coordinate rates, as shown in Eq. (12).

$$\begin{bmatrix} \omega_x \\ \omega_y \\ \omega_z \end{bmatrix} = \begin{bmatrix} -\sin o_2 & 0 & 1 \\ \cos o_2 \sin o_1 & \cos o_1 & 0 \\ \cos o_2 \cos o_1 & -\sin o_1 & 0 \end{bmatrix} \begin{bmatrix} \dot{o}_3 \\ \dot{o}_2 \\ \dot{o}_1 \end{bmatrix} \tag{12}$$

$$\omega_x \approx \dot{o}_1$$
$$\text{if} \quad o_1, o_2 \ll 1 \quad \text{then} \quad \omega_y \approx \dot{o}_2$$
$$\omega_z \approx \dot{o}_3$$

2.4. External forcing and static deflection

In this paper, a very simple model of the effect of the SRP on each blade segment is set to only consider the specular component of the reflection, while secondary effects, such as albedo or self-illumination are ignored. SRP is assumed to be incident along the spinning-axis of the hub (body) frame.

Equation 13 is used to approximate the SRP influence along the normal for each segment, where the quantity e_i is the incident SRP vector (pegged to e_Z, the spinning axis of the hub frame), e_n is the unit normal at an arbitrary point on the segment surface, and α represents the smallest angle between them.

$$f_n = -f_{srp}(\cos^2\alpha)e_n = -f_{srp}(e_i \cdot e_n)^2 e_n \qquad (13)$$

Because this is a discrete-mass model, the SRP is assumed to be equally distributed on each of the point masses. The external torque with respect to each generalized coordinate is found by applying the principle of virtual work, as shown in Eq. (14),

$$\tau_q = \sum_{i=1}^{n}\left(f_{ni}\cdot\frac{\delta R1_i}{\delta q} + f_{ni}\cdot\frac{\delta R2_i}{\delta q}\right) \qquad (14)$$

where $R1$ and $R2$ correspond to the 1st and 2nd of the point mass pairs at the end, or beginning, of each blade segment.

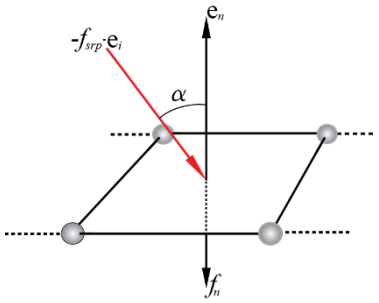

Fig. 4. Diagram of SRP influence on blade surface

As the entire heliogyro structure spins up, the centrifugal force generated by the rotation will, at some point, reach equilibrium with the normal force that the SRP exerts on each blade. This state of static deflection is obtained by setting all displacement variables –other than out-of-plane bending-- and derivatives to zero, equating with the SRP forcing, and solving for the permanent out-of-plane bending (w_s). In Eq. (15), this operation would natural cancel any terms in the nonlinear mass matrix (M_n).

$$M_n(q)[\ddot{q} \quad \dot{\omega}]^T + K_n(q,\dot{q},\omega)\big|_{\substack{w=w_s+\Delta w\\ \omega=\omega_0+\Delta\omega}} = \tau_q\big|_{\substack{w=w_s+\Delta w\\ \omega=\omega_0+\Delta\omega}} \qquad (15)$$

Similarly, the rotation about the e_Z-axis in the body frame is set to follow a constant rpm value (ω_0), around which variations are allowed ($\Delta\omega$). The analysis performed in this paper is carried out on the linearized system around these constant states.

3. Stability Analysis

In order to understand the stability characteristics of the solar sail, it is necessary to study the relation between the spacecraft's flight conditions and the corresponding dynamic response of the blades. Although other parameters that would affect stability can also be studied, it is evident that the single most important factor affecting performance is the amount of SRP the heliogyro is under. Therefore, this manuscript limits itself to studying the changing stability conditions of the heliogyro under differing amounts of SRP, which is, in other words, a study of the relation between structural stability and distance to the Sun. Table 1 shows some of the chosen simulation parameters. The effects of varying additional parameters such as the hub dimensions will also be discussed.

Table 1. Structural parameters

Blade density	1490 kg/m^3
Hub mass (m_h)	7.6 kg
Blade length	220 m
Blade width	0.75 m
Blade thickness	2.74x10^{-6} m

It is important to note that, although it is clear that the chosen representation of the blade as a system of interconnected masses is physically incompatible with parameters such as the axial and torsional stiffness, E, and G, commonly associated with beam theory; the goal of the approach is to develop a model which best conforms to known results from more rigorous approaches. Thus, the stiffness values are chosen so that the resulting simulations approach previous observations. Future studies should focus on deriving a rigorous way of assigning stiffness parameters to the proposed model.

The simulations that follow are derived from models that attempt to maximize the number of segments to represent each blade, while maintaining the computational load reasonable, which is itself a subject of future research. The spinning rate for all simulations is set to 1 rpm, and the models are linearized about that value, which is the nominal spin rate given in the HELIOS mission parameters.

3.1. Single rotating blade

Figure 5 depicts the frequency variation of a single blade under constant 1 rpm rotation about the e_z axis, with no hub, under the effect of increasing solar radiation pressure. In concordance with previous research,[11,12] the model exhibits coupling between the in-plane (v) and twisting (φ) modes as their corresponding frequencies coalesce into a flutter instability (red curve), which is, in other words, a fundamentally uncontrollable excitation of the structural modes. A divergence instability (blue curve) also takes place at higher levels of SRP. In the figure, the first twisting modes' corresponding frequency ratio begins near 1.4, while that of the first in-plane mode starts at 0.5. The out-of-plane modes' frequency ratios appear as straight lines along all SRPs, because it lacks coupling with other blade motions.

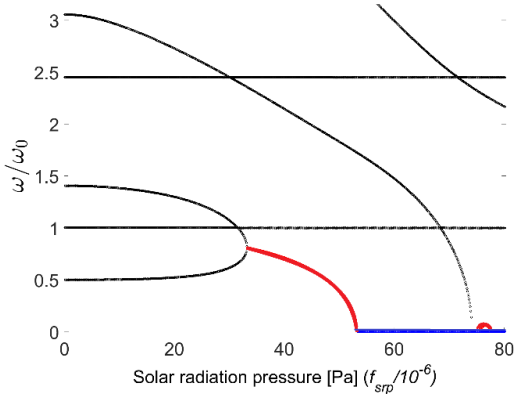

Fig. 5. Normalized frequencies (1 blade, no hub, constant spin)

By recording the single blade system's first onset of flutter with increasing number of approximating segments, and assuming increased fidelity, it is possible to forecast the flutter conditions of the system. Figure 6 shows that, increasing the number of approximating segments in the model, describes an asymptotical trend (blue line) that converges toward the SRP value of 30×10^{-6} Pa at 1 rpm of spinning rate. If a perfectly reflective blade surface is assumed, this would correspond to 0.545AU –nearly halfway to the sun. Although this result differs from the flutter onset SRP projected in previous NASA studies [18] (~40×10^{-6} Pa), several corrective steps can be taken to close this gap. This includes, as was mentioned previously, developing a more rigorous derivation of the stiffness parameters for the model, which inherently affect the flutter conditions.

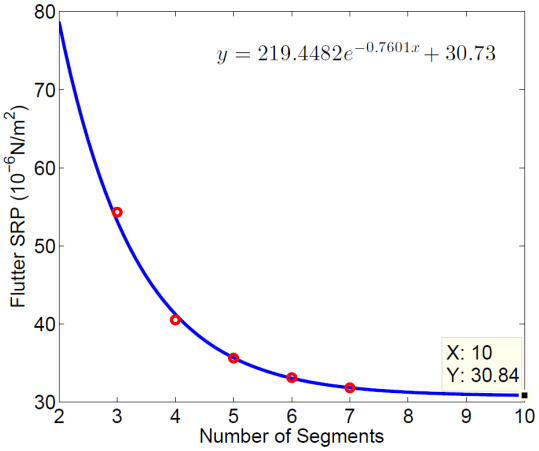

Fig. 6. Projection of flutter onset SRP at 1 rpm [source: ref. (9)]

3.2. 1 blade + hub

The addition of a hub provides some stabilization to the spinning structure, as it carries most of the rotational inertia of the system. This is shown in figure 7, where divergence-type instability occurs at a greater value of SRP than that of the previous example. The model used to produce the figure is linearized around the nominal 1 rpm spin rate, and allowed to freely spin up or down from that value.

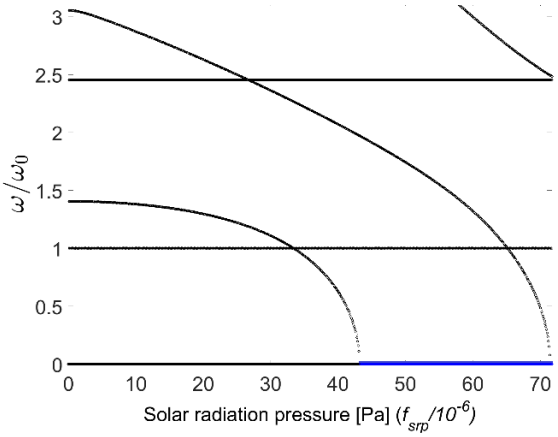

Fig. 7. Normalized frequencies (1 blade + hub, free spin)

It is evident that the instabilities of the system are manifested differently due to the addition of the hub. The first twisting modes, with corresponding frequency ratio starting around 1.4 in figure 7, no longer converge with the first in-plane modes of the blade. Essentially, in a freely spinning structure, the in-plane modes of the blade will be subsumed by the rotation of the hub about the body z-axis, thus making the coupling between in-plane and twisting blade motions to yield to coupling between body rotations and the blade's twisting motion. This becomes a recurring phenomenon in all models, and it suggests that active actuation, such as reaction wheel control, is necessary at the hub in order to prevent large, sudden hub rotations to couple with the modes of the blades.

3.2. 2 blades + hub

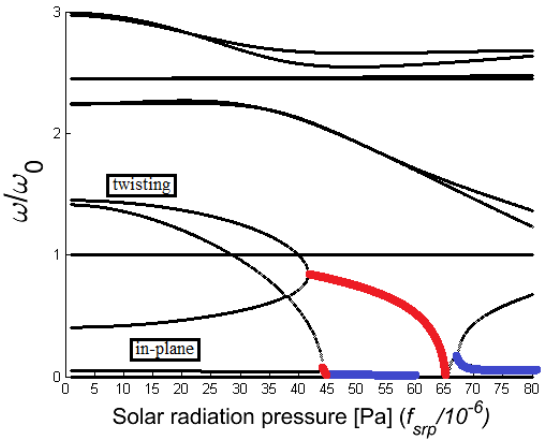

Fig. 8. Normalized frequencies (2 blade + hub, free spin)

The frequencies in figure 8 show flutter occurring in separate instances as the blade's twisting frequencies (starting at a frequency ratio near 1.4) converge to the in-plane frequencies. The two twisting frequencies that start near 1.4 on the y-axis of the figure and the two in-plane frequencies that immediately precede a ratio of 1, are both symmetric and antisymmetric modes of the twisting, and in-plane motions, respectively. The distinction is made because, even though the eigenvectors of the system change as their respective frequencies progress through the figure, the initial conditions of the system could determine where and how the blades reach instability.

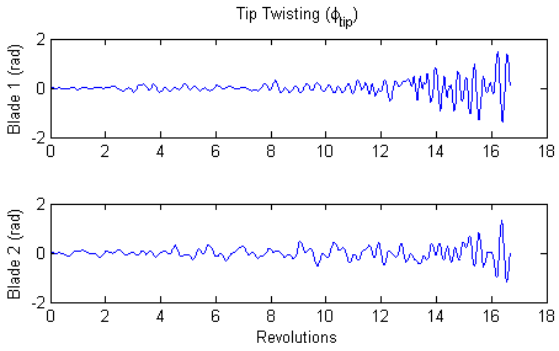

Fig. 9. Tip flutter (2 blade + hub, free spin)

Figure 9 shows the evolution of the tip's twist angle at a 43×10^{-6} Pa level of SRP. This simulation is obtained through integration of the exact set of nonlinear equations of motion according to the proposed model using small initial conditions. The uncontrolled excitation of the twisting at the tip –which we refer to as 'flutter'— is shown here to occur as it was anticipated in the analysis of the linear modes. These results for the two-blade heliogyro are in concordance with current studies being carried out at NASA under other modeling approaches.

3.3. 4 blades + hub

The four-blade heliogyro simulation in figure 10 shows that the twisting modes encounter divergence instabilities, as opposed to converging to flutter conditions with the in-plane modes. The SRP value at the onset of instability is shown to be near 35×10^{-6} Pa, noticeably lower than in previous simulations.

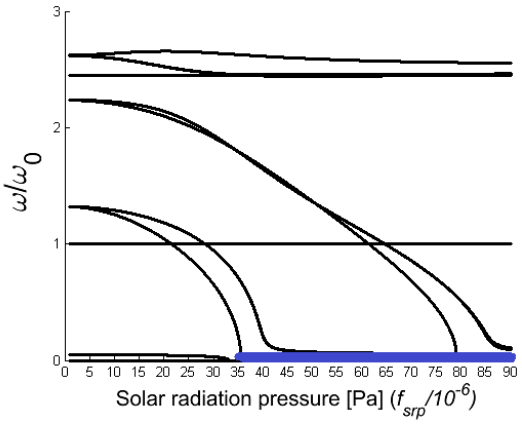

Fig. 10. Normalized frequencies (4 blade + hub, free spin)

3.4. Hub sizing

While the occurrence of flutter is always dependent on the stiffness properties of the system, as one would expect, instabilities may onset at smaller levels of SRP if care is not taken to properly size the hub.

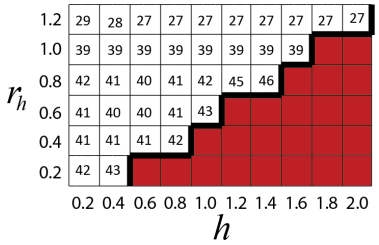

Fig. 11. Flutter onset SRP vs. hub size parameters (2-blades+hub)

Figure 11 charts the amount of SRP at the first onset of flutter as a function of the hub radius, r_h, and height, h, for the two-blade model. Results suggest that, for the two-blade model, if the shape of the hub is taken to be roughly cylindrical, then smaller diameter, and larger height offer the best performance. In the figure, the colored area represents size combinations which yield instability at all SRP levels.

The four-blade heliogyro is, as expected, a more stable platform than the two-blade system. A similar analysis shows the same trend regarding the hub's diameter, while the height of the hub is shown to have no effect on the structure's stability.

4. Conclusions

The paper shows a hybrid approach to derive equations of motion for a heliogyro structure with a rigid body hub, and a lumped-mass approximation of the blade. The latter incorporated elements of beam theory in order to formulate potential energies. The generalized force contribution from SRP is formulated for the system, upon which static deflection conditions are determined.

The model shows promising results in approximating the flutter conditions of the system, and in reproducing the manner in which these flutter conditions are reached, as compared with current NASA results.[18] The four-blade heliogyro is shown to achieve an unstable condition in a differing manner than that of its two-blade counterpart. Additionally, the necessity to properly size the hub in order to influence the range of stable operations is shown in a simple trade study.

Further refinements, such as devising a rigorous manner of obtaining the blade stiffness parameters for each n-segment approximation of the blade, is necessary to validate these results.

References

1) R. MacNeal. *Structural Dynamics of the Heliogyro*. NASA Contractor Report CR 1745A, 1971.
2) D.H. Hodges and E.H. Dowell. *Nonlinear Equation of Motion for the Elastic Bending and Torsion of Twisting Nonuniform Rotor Blades*. NASA Technical Note D-7818, 1974.
3) S.C. Gibbs IV and E.H. Dowell. "Solarelastic Stability of the Heliogyro." Advances in Solar Sailing, pages 651-665, 2014.
4) M. Natori and S. Nemat-Nasser. "Application of a Mixed Variational Approach to Aeroelastic Stability Analysis of a Nonuniform Blade." Journal of Struct. Mechanics, 5-31, 1986.
5) M. Natori, S. Nemat-Nasser, and J. Mitsugi. "Instabiliy of a Rotating Blade Subjected to Solar Radiation Pressure." AIAA Structure, Struct. Dynamics, and Materials Conf., Apr. 1989.
6) A. Scholz, T.H. Hsiao, and J. Juang. "Design and Analysis of Heliogyro Sail Deployment System." In Proceedings of the 13th European Conference of Spacecraft Structures, Materials and Environmental Testing, Braunschweig, Germany, April, 2014.
7) J. Juang, C. Hung, and K. Wilkie. "Dynamics of a Spinning Membrane." In AAS Jer-Nan Juang Astrodynamics Symposium. Paper 2012-601, College Station, TX, June 2012.
8) Y. Huang, J. Juang, C. Hung, and K. Wilkie. "Dynamics of a Coupled Pendulum Model of a Heliogyro Membrane Blade." In 3rd Int'l Symposium on Solar Sailing, Glasgow, UK. June 2012.
9) L.W. Tsai. *Stability Analysis and Dynamic Response of a Membrane Blade of Heliogyro Solar Sail*. M.S. Thesis, National Cheng Kung University, Tainan City, Taiwan. 2016.
10) L.W. Tsai, A. Pimienta-Peñalver, J.L. Crassidis, and J. Juang. "Dynamics of a Spinning Structure Subjected to Uniform Pressure". In 6th International Conference on High Performance Scientific Computing. Paper 31, Hanoi, Vietnam, March 2015.
11) R. Meirovitch. "Hybrid state equations of motion for flexible bodies in terms of quasi-coordinates." Journal of Guidance, Control, and Dynamics, 14. 1008-1013, 1991.
12) R. Blomquist. *Heliogyro Control*. Dissertation, The Robotics Institute, Carnegie Mellon University, 2009.
13) J. Juang, H. Lu, L. Horta, and K. Wilkie. "Challenges Associated with System Identification and Control of a Heliogyro Membrane Blade." In Advances in Solar Sailing, 705-716. Springer, Hanoi, Vietnam, 2014.
14) D. Guerrant, D. Lawrence, and K. Wilkie. "Heliogyro Solar Sail Blade Twist Control." In 35th Annual AAS Guidance and Control Conference, Breckenridge, CO, February 2012.
15) D. Guerrant, K. Wilkie, and D. Lawrence. "Heliogyro Blade Twist Control via Reflectivity Modulation." In 13th AIAA Gossamer Systems Forum, 23-26, Honolulu, HI, April, 2012.
16) D. Guerrant and D. Lawrence. "Tactics for Heliogyro Solar Sail Attitude Control via Blade Pitching." Journal of Guidance, Control, and Dynamics, 1-15, 2015.
17) D. Guerrant. *Performance Quantification of Heliogyro Solar Sails Using Structural, Attitude, and Orbital Dynamics and Control Analysis*. Dissertation, University of Colorado, 2015.
18) K. Wilkie et al. "Heliogyro Solar Sail Research at NASA." In 3rd Int'l Symposium on Solar Sailing, Glasgow, UK. June 2012.